Supplementary Material to: Hydrodynamic dispersion in Hele-Shaw flows with inhomogeneous wall boundary conditions

Sebastian Dehe[1], Imke-Sophie Rehm[1], and Steffen Hardt[1]

[1]*Fachbereich Maschinenbau, Technische Universität Darmstadt, 64287 Darmstadt, Germany*

S1 Comparison to 2D Taylor-Aris dispersion coefficients

S1.1 Plane Poiseuille flow

Here we reproduce the well-known case of a purely pressure-driven flow between two infinite plates. We assume vanishing boundary slip everywhere ($\beta = 0$) and the flow to be unidirectional in the x-direction. The non-dimensionalized flow field is given by

$$u = -\frac{1}{2}z(1-z)\frac{\partial p}{\partial x}, \tag{1a}$$

$$u - \langle u \rangle = \left(\frac{1}{2}z^2 - \frac{1}{2}\frac{\partial p}{\partial x}z + \frac{1}{12}\right)\frac{\partial p}{\partial x}, \tag{1b}$$

$$a = \left(\frac{1}{24}z^4 - \frac{1}{12}z^3 + \frac{1}{24}z^2 - \frac{1}{720}\right)\frac{\partial p}{\partial x}, \tag{1c}$$

where the problem 2.24 was solved for the given flow field 1a. Finally, we obtain the dispersion coefficient as

$$\langle ua \rangle = -\frac{\left(\frac{\partial p}{\partial x}\right)^2}{30240} = -\frac{\langle u \rangle^2}{210}, \tag{2}$$

where we have used the average velocity to cast the dispersion coefficient in a more familiar form. This expression agrees with the one from the literature Wooding (1960).

S1.2 Couette flow

A second instructive case is the flow induced by an electric field, with a constant electroosmotic mobility on one wall of a parallel-plates geometry without any external pressure, representing a channel with open ends. A shear flow with the classical Couette profile will develop, and the dispersion coefficient can be computed in a similar manner as in the previous section. We non-dimensionalize the flow field with the wall velocity as the characteristic velocity scale, and obtain

$$u = z, \tag{3a}$$

$$u - \langle u \rangle = z - \frac{1}{2}, \tag{3b}$$

$$a = \frac{1}{6}z^3 - \frac{1}{4}z^2 + \frac{1}{24}, \tag{3c}$$

The dispersion coefficient is then given by

$$\langle ua \rangle = -\frac{1}{120} = -\frac{\langle u \rangle^2}{30}, \tag{4}$$

where we have used the average velocity to cast the dispersion coefficient in a more familiar form. This form again coincides with an expression from the literature (Balakotaiah *et al.*, 1995). On a second note, the dispersion in a pure shear flow is enhanced significantly compared to a pressure-driven flow with the same average velocity. Later on, we will see the importance of this observation.

S2 Alternative derivation of dispersion model for the stationary case

In this section, we derive the dispersion model for the case of stationary flow using scaling arguments, outlining the analogy to other work considering hydrodynamic dispersion. First, we rewrite the dimensional advection-diffusion equation based on the wall-parallel and wall-normal components of the nabla operator as

$$\frac{\partial c}{\partial t} + \boldsymbol{u}_{\parallel} \cdot \boldsymbol{\nabla}_{\parallel} c + \boldsymbol{u}_{\perp} \cdot \boldsymbol{\nabla}_{\perp} c = \boldsymbol{\nabla}_{\parallel} \cdot \left(D \boldsymbol{\nabla}_{\parallel} c \right) + \boldsymbol{\nabla}_{\perp} \cdot \left(D \boldsymbol{\nabla}_{\perp} c \right) . \tag{5}$$

In the next step, we split the concentration into an height-averaged value and a variation part, and non-dimensionalize, leading to an expression for the concentration field as

$$c = \langle c \rangle + \Delta c \left(z \right) = c_0 \langle \hat{c} \rangle + \Delta c_0 \Delta \hat{c} \left(\hat{z} \right) , \tag{6}$$

where the height-averaged concentration scale is denoted by c_0 and the scale of the variation by Δc_0. Hatted symbols denote non-dimensional quantities. The corresponding forms of the parallel and normal velocities are

$$\boldsymbol{u}_{\parallel} \left(z \right) = \langle \boldsymbol{u}_{\parallel} \rangle + \boldsymbol{\Delta u}_{\parallel} \left(z \right) = U_c \langle \hat{\boldsymbol{u}}_{\parallel} \rangle + U_c \boldsymbol{\Delta} \hat{\boldsymbol{u}}_{\parallel} \left(z \right) \tag{7}$$

and

$$\boldsymbol{u}_{\perp} \left(z \right) = \langle \boldsymbol{u}_{\perp} \rangle + \boldsymbol{\Delta u}_{\perp} \left(z \right) = W_c \langle \hat{\boldsymbol{u}}_{\perp} \rangle + W_c \boldsymbol{\Delta} \hat{\boldsymbol{u}}_{\parallel} \left(z \right) . \tag{8}$$

It is important to note that we assume that the scale of the velocity is of the same order as the variation of the velocity over the channel height, thus only leading to the scales U_c and W_c.

As in the previous derivation, we drop the hats in the following for readability, using only non-dimensionalized quantities. In order to derive an equation for the height-averaged concentration $\langle c \rangle$, we insert equations 6, 7 and 8 into the non-dimensionalized advection-diffusion equation 5 and average over the channel height, leading to

$$\frac{\partial \langle c \rangle}{\partial t} + \epsilon Pe \left(\langle \boldsymbol{u}_{\parallel} \rangle \cdot \boldsymbol{\nabla}_{\parallel} \langle c \rangle + \frac{\Delta c_0}{c_0} \langle \boldsymbol{\Delta u}_{\parallel} \cdot \boldsymbol{\nabla}_{\parallel} \Delta c \rangle + \frac{\Delta c_0}{c_0} \langle \boldsymbol{\Delta u}_{\perp} \cdot \boldsymbol{\nabla}_{\perp} \Delta c \rangle \right) = \epsilon^2 \boldsymbol{\nabla}_{\parallel}^2 \langle c \rangle . \tag{9}$$

In this equation, the height-averages over the product of the variations are not known and need to be calculated.

We can generate an equation for the concentration variations by subtracting 9 from the advection-diffusion equation 5, leading to

$$\begin{aligned} \frac{1}{Pe} \frac{\partial \Delta c}{\partial t} + \epsilon \Bigg(& \frac{c_0}{\Delta c_0} \boldsymbol{\Delta u}_{\parallel} \cdot \boldsymbol{\nabla}_{\parallel} \langle c \rangle \\ & + \langle \boldsymbol{u}_{\parallel} \rangle \cdot \boldsymbol{\nabla}_{\parallel} \Delta c + \langle \boldsymbol{u}_{\perp} \rangle \cdot \boldsymbol{\nabla}_{\perp} \Delta c + \boldsymbol{\Delta u}_{\parallel} \cdot \boldsymbol{\nabla}_{\parallel} \Delta c + \boldsymbol{\Delta u}_{\perp} \cdot \boldsymbol{\nabla}_{\perp} \Delta c \Bigg) \\ & = \frac{1}{Pe} \left[\epsilon^2 \boldsymbol{\nabla}_{\parallel}^2 \Delta c + \boldsymbol{\nabla}_{\perp}^2 \Delta c \right] + \epsilon \langle \boldsymbol{\Delta u}_{\parallel} \cdot \boldsymbol{\nabla}_{\parallel} \Delta c \rangle + \epsilon \langle \boldsymbol{\Delta u}_{\perp} \cdot \boldsymbol{\nabla}_{\perp} \Delta c \rangle . \end{aligned} \tag{10}$$

In order to balance the different terms in this equation, we find that $\Delta c_0 / c_0$ is of order ϵPe. Otherwise the second terms on both sides of the equation would not be balanced. As a result, the lowest order in ϵ reads

$$\epsilon Pe \frac{c_0}{\Delta c_0} \boldsymbol{\Delta u}_{\parallel} \cdot \boldsymbol{\nabla}_{\parallel} \langle c \rangle \approx \boldsymbol{\nabla}_{\perp}^2 \Delta c . \tag{11}$$

Expression 11 describes the concentration variation over the channel height, and since we have expressions for the flow field $\boldsymbol{\Delta u}_{\parallel}$ from Appendix B, we can express the concentration variation as a function of the velocity variation over the channel height.

The expression for $\boldsymbol{\Delta u}_{\parallel}$ can be derived by subtracting the equation for the averaged flow velocity B8 from that for the total velocity B5. In a general form, without expressing the velocity explicitly, it can be written as a second-order polynomial

$$\boldsymbol{\Delta u}_{\parallel} = \boldsymbol{A}_u = \boldsymbol{A}_1 z^2 + \boldsymbol{A}_2 z + \boldsymbol{A}_3 . \tag{12}$$

Inserting equation 12 in equation 11 and integrating twice with respect to z, the concentration variation can be expressed as

$$\begin{aligned}\Delta c &= \epsilon Pe \frac{c_0}{\Delta c_0} \boldsymbol{\nabla}_\parallel \langle c \rangle \cdot \int_0^z \int_0^z \boldsymbol{\Delta u}_\parallel \mathrm{d}\tilde{z}\mathrm{d}\tilde{z} \\ &= \epsilon Pe \frac{c_0}{\Delta c_0} \boldsymbol{\nabla}_\parallel \langle c \rangle \cdot \left(\frac{1}{12}\boldsymbol{A}_1 z^4 + \frac{1}{6}\boldsymbol{A}_2 z^3 + \frac{1}{2}\boldsymbol{A}_3 z^2 + \boldsymbol{A}_4 z + \boldsymbol{A}_5 \right).\end{aligned} \tag{13}$$

The impermeable wall condition leads to $\partial \Delta c / \partial z = 0$, therefore $\boldsymbol{A}_4$ has to vanish. If we compare this equation with equations 2.23 and 2.24, the analogy to the first-order perturbation becomes apparent: Δc is obtained as a product of a double integral over the velocity variation and the gradient of the height-averaged velocity $\boldsymbol{\nabla}_\parallel \langle c \rangle$ (equation 13). In the perturbation approach, $c^{(1)}$ is obtained as a product of $\boldsymbol{a}$, which is defined as a double integral over the velocity variation (equation 2.24) , and the gradient of the average concentration $\boldsymbol{\nabla}_\parallel c^{(0)}$ (equation 2.23). It is important to note that the defining equation for $\boldsymbol{a}$ in the multiscale pertubation approach arises from the systematic analysis of the equations, whereas in this derivation, it is a direct result of the order-of-magnitude argument 11.

Now that we have a solution for the concentration variation over the channel height, we can assemble the expressions for the final transport equation 9. We obtain

$$\begin{aligned}\langle \boldsymbol{\Delta u}_\parallel \cdot \boldsymbol{\nabla}_\parallel \Delta c \rangle &= \epsilon Pe \frac{c_0}{\Delta c_0} \int_{z=0}^1 \boldsymbol{\Delta u}_\parallel \cdot \boldsymbol{\nabla}_\parallel \left[\left(\frac{1}{12}\boldsymbol{A}_1 z^4 + \frac{1}{6}\boldsymbol{A}_2 z^3 + \frac{1}{2}\boldsymbol{A}_3 z^2 + \boldsymbol{A}_5 \right) \cdot \boldsymbol{\nabla}_\parallel \langle c \rangle \right] \mathrm{d}z \\ &= \epsilon Pe \frac{c_0}{\Delta c_0} \int_{z=0}^1 \boldsymbol{\Delta u}_\parallel \mathrm{d}z \cdot \boldsymbol{\nabla}_\parallel \left(\boldsymbol{A}_5 \cdot \boldsymbol{\nabla}_\parallel \langle c \rangle \right) \\ &+ \epsilon Pe \frac{c_0}{\Delta c_0} \int_{z=0}^1 \boldsymbol{\Delta u}_\parallel \cdot \boldsymbol{\nabla}_\parallel \left[\left(\frac{1}{12}\boldsymbol{A}_1 z^4 + \frac{1}{6}\boldsymbol{A}_2 z^3 + \frac{1}{2}\boldsymbol{A}_3 z^2 \right) \cdot \boldsymbol{\nabla}_\parallel \langle c \rangle \right] \mathrm{d}z,\end{aligned} \tag{14}$$

where the first term after the last equal sign is zero by definition, since the integral over the channel height of the velocity deviation $\langle \boldsymbol{\Delta u}_\parallel \rangle$ vanishes. Further, we introduce the abbreviation $\boldsymbol{a} = \frac{1}{12}\boldsymbol{A}_1 z^4 + \frac{1}{6}\boldsymbol{A}_2 z^3 + \frac{1}{2}\boldsymbol{A}_3 z^2$, resulting in

$$\begin{aligned}\langle \boldsymbol{\Delta u}_\parallel \cdot \boldsymbol{\nabla}_\parallel \Delta c \rangle &= \epsilon Pe \frac{c_0}{\Delta c_0} \int_{z=0}^1 \boldsymbol{\Delta u}_\parallel \cdot \boldsymbol{\nabla}_\parallel \left(\boldsymbol{a} \cdot \boldsymbol{\nabla}_\parallel \langle c \rangle \right) \mathrm{d}z \\ &= \epsilon Pe \frac{c_0}{\Delta c_0} \int_{z=0}^1 \Delta u \left(a_x \frac{\partial^2 \langle c \rangle}{\partial x^2} + a_y \frac{\partial^2 \langle c \rangle}{\partial x \partial y} \right) + \Delta v \left(a_x \frac{\partial^2 \langle c \rangle}{\partial x \partial y} + a_y \frac{\partial^2 \langle c \rangle}{\partial y^2} \right) \\ &+ \Delta u \left(\frac{a_x}{\partial x} \frac{\langle c \rangle}{\partial x} + \frac{a_y}{\partial x} \frac{\langle c \rangle}{\partial y} \right) + \Delta v \left(\frac{a_x}{\partial y} \frac{\langle c \rangle}{\partial x} + \frac{a_y}{\partial y} \frac{\langle c \rangle}{\partial y} \right) \mathrm{d}z,\end{aligned} \tag{15}$$

where the subscripts x, y indicate vector components in the x- and y-direction, respectively.

The term $\langle \boldsymbol{\Delta u}_\perp \cdot \boldsymbol{\nabla}_\perp \Delta c \rangle$ can be expressed as

$$\langle \boldsymbol{\Delta u}_\perp \cdot \boldsymbol{\nabla}_\perp \Delta c \rangle = \epsilon Pe \frac{c_0}{\Delta c_0} \boldsymbol{\nabla}_\parallel \langle c \rangle \cdot \left\langle \Delta w \frac{\partial \boldsymbol{a}}{\partial z} \right\rangle. \tag{16}$$

Finally, we can write the final transport equation as

$$\frac{\partial c}{\partial t} + \left[\epsilon Pe \langle \boldsymbol{u}_\parallel \rangle \cdot \boldsymbol{\nabla}_\parallel \langle c \rangle - \epsilon^2 Pe \boldsymbol{k}_c \cdot \boldsymbol{\nabla}_\parallel \langle c \rangle \right] = \epsilon^2 \boldsymbol{\nabla}_\parallel \cdot \left[\left(\boldsymbol{I} - Pe^2 \boldsymbol{D} \right) \cdot \boldsymbol{\nabla}_\parallel \langle c \rangle \right], \tag{17}$$

where $\boldsymbol{k}_c$ denotes an advection-correction term, $\boldsymbol{I}$ the identity matrix, and $\boldsymbol{D}$ the dispersion tensor. The advection-correction term is given as

$$\boldsymbol{k}_c = \begin{bmatrix} \left\langle \frac{\partial \Delta u_x}{\partial x} a_{,x} \right\rangle + \left\langle \frac{\partial \Delta u_x}{\partial y} a_{,x} \right\rangle - \left\langle w \frac{\partial a_x}{\partial z} \right\rangle \\ \left\langle \frac{\partial \Delta u_y}{\partial x} a_{,y} \right\rangle + \left\langle \frac{\partial \Delta u_y}{\partial y} a_{,y} \right\rangle - \left\langle w \frac{\partial a_y}{\partial z} \right\rangle \end{bmatrix}, \tag{18}$$

and the dispersion tensor by

$$\boldsymbol{D} = \begin{bmatrix} \langle \Delta u a_x \rangle & \langle \Delta u a_y \rangle \\ \langle \Delta v a_x \rangle & \langle \Delta v a_y \rangle \end{bmatrix}. \tag{19}$$

The equivalence to the macrotransport equation can be shown by disregarding the oscillatory components in equation 2.29.

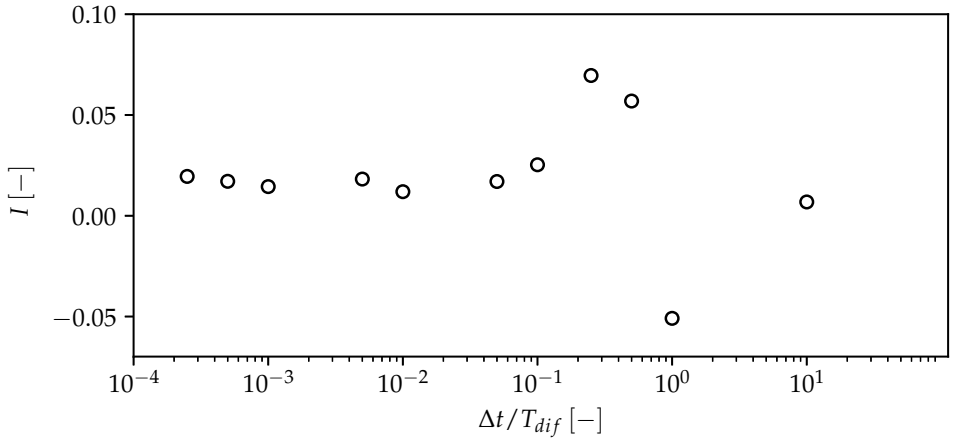

Figure 1: Convergence study with respect to the maximum time step size in the particle-tracking simulations. The mixing intensity is evaluated after $t = 872.9\,T_{\mathrm{dif,h}}$.

S3 Additional information related to the 3D particle simulations

As becomes evident from equation D1, the time-step size has a strong influence on the random force acting on a particle. It is important that the time steps are small enough for particles to react to the force sufficiently often during a time interval given by the cross-stream diffusion time. Therefore, the time stepping scheme has to fulfill the condition $\Delta t \ll T_{\mathrm{dif,h}}$. We have performed a convergence study with a recirculating flow field, similar to what we considered in 5.4, with similar cell height of $h = 100\,\mu$m, a molecular diffusion constant of $D = 1 \times 10^{-10}\,\mathrm{m}^2/\mathrm{s}$ and a maximum velocity of $500\,\mu$m/s, where we have varied the maximum time step size. We used the *Generalized alpha* solver, which is an implicit, second-order accurate time-stepping scheme with less numerical damping of high-frequency components than comparable implicit solvers. We fixed the maximum time step Δt to a case-specific value and chose a *High frequency amplification factor* of 0.75. When running a simulation we used a *relative tolerance* of 10^{-3}.

In order to perform a convergence study, we implemented a global measure for mixing as

$$I = 1 - \frac{\int \left| c(t) - c_{\mathrm{avg}} \right| \mathrm{d}V}{\int \left| c(0) - c_{\mathrm{avg}} \right| \mathrm{d}V}, \tag{20}$$

where c_{avg} denotes the average concentration over the computational domain, and c the concentration at a specific location and time. This measure will vary from 0 at the initial time to 1 when complete mixing is achieved. In order to compute the global measure, we compute the particle count per cell, and transform it to a concentration distribution. The concentration can be computed by normalizing the local particle number density at a specific point in time with the initial particle number density obtained for a known concentration, for example in the region of maximum concentration at the initial timestep.

The results for the mixing intensity as a function of the non-dimensionalized maximum time step size are shown in figure 1. As is visible, for values close to the diffusive timescale $T_{\mathrm{dif,h}}$, the results are unphysical and strongly oscillate, leading to de-mixing. For values much smaller, the mixing intensity converges to an asymptotic value. This means that from a specific point on, a further decrease of the maximum time step size does not significantly change the results. As final value we have chosen $\Delta t = 2.5 \times 10^{-4}\,T_{\mathrm{dif,h}}$, thus ensuring sufficient resolution of the diffusion processes.

S4 Additional information related to the numerical solution of the 2D dispersion model

In this section, we provide additional information about the numerical implementation of the 2D model in Comsol Multiphysics 5.5. As in the preceding section, information regarding specific settings used in Comsol is indicated by

italic fonts.

The flow equations are implemented in Comsol using a *convection-diffusion equation interface*, where we solve for the pressure distribution inside the cell (equation 3.5). The governing equations are given in section 3. At the perimeter of the parallel-plates domain, we can apply either Dirichlet boundary conditions for the pressure ($p = p_0$) or no-penetration boundary conditions. The latter are given by $\langle \boldsymbol{u}_{\parallel} \rangle \cdot \boldsymbol{n} = 0$, where $\boldsymbol{n}$ denotes the normal vector of the boundary at the perimeter. According to equation B8 this leads to

$$\boldsymbol{n} \cdot \left(-\frac{1}{12} \langle \mu^{\mathrm{p}} \rangle \boldsymbol{\nabla}_{\parallel} p + \langle \mu^{\mathrm{EOF}} \rangle \boldsymbol{E}_{\parallel} \right) = 0. \tag{21}$$

In addition, to render the pressure unique, it has to be fixed at one point on the boundary to prevent numeric oscillations. Also, we utilized the in-built stabilization scheme (*consistent stabilization with streamline and crosswind diffusion*, (COMSOL Multiphysics, 2019)). To ensure that the mesh is fine enough to suppress numerical diffusion, the results of a mesh refinement study are reported below (see figure 2).

The distribution of the wall mobility in test case C is given by

$$\begin{aligned} \mu_{\mathrm{EOF}}^{L} =& \mu_0 \, R(x/2, L_{\mathrm{smooth,x}}) \, R\left(y - \frac{L_{\mathrm{patch}} - L_{\mathrm{smooth,y}}}{2}, L_{\mathrm{smooth,y}} \right) \\ & - R(x/2, L_{\mathrm{smooth,x}}) \, R\left(y + \frac{L_{\mathrm{patch}} + L_{\mathrm{smooth,y}}}{2}, L_{\mathrm{smooth,y}} \right), \end{aligned} \tag{22}$$

where R is a smoothed step function, defined as $R(x, L_{\mathrm{smooth}}) = H(x + L_{\mathrm{patch}}/2, L_{\mathrm{smooth}}) - H(x - L_{\mathrm{patch}}/2, L_{\mathrm{smooth}})$, where $H(x, d)$ is a smoothed Heaviside function with continuous second derivative:

$$H(x,d) = \begin{cases} 0 & \text{if } x < -d \\ 0.5 + 0.9375\frac{x}{d} - 0.625\left(\frac{x}{d}\right)^3 + 0.1875\left(\frac{x}{d}\right)^5 & \text{if } -d < x < d \\ 1 & \text{if } x > d. \end{cases} \tag{23}$$

The resulting wall-mobility distribution is shown in figure 9(b). For solving the flow equations, we utilize *MUMPS*, a direct solver, with a *relative tolerance* of 1×10^{-3}.

For the discretization of the pressure, elements of quartic order are chosen to ensure sufficient resolution at the level of individual mesh cells. The mesh consists of triangular cells, where we only restrict the maximum size of the elements and the meshing is performed automatically by Comsol. The final mesh utilized in test case C consists of 73138 triangles with a *minimum element quality* of 0.666 and an *average element quality* of 0.9698. We performed convergence studies, as discussed below. The obtained velocity fields serve as input for the 3D particle tracking simulations, among others.

From the obtained pressure field, we compute the coefficients in the macrotransport equation according to equations 2.30 - 2.32. These coefficients are then implemented in the advection-diffusion equation, where we solve for $c^{(0)}$. Here, we utilized elements of quadratic order. At the boundaries, we can prescribe a no-flux condition. The concentration field is solved for on a similar mesh as for the flow, and the corresponding convergence study is shown below. For test cases A and B, we assigned an initial concentration distribution as

$$c_0(t=0) = \frac{1}{2}\left[1 + \mathrm{erf}\left(\frac{x - y_{\mathrm{off}}}{L_{\mathrm{c,ini}}}\right)\mathrm{erf}\left(\frac{-x - y_{\mathrm{off}}}{L_{\mathrm{c,ini}}}\right)\right]\left[1 + \mathrm{erf}\left(\frac{y - y_{\mathrm{off}}}{L_{\mathrm{c,ini}}}\right)\mathrm{erf}\left(\frac{-y - y_{\mathrm{off}}}{L_{\mathrm{c,ini}}}\right)\right], \tag{24}$$

where erf() denotes the error function, and we chose $y_{\mathrm{off}} = 1250\,h$ and $L_{\mathrm{c,ini}} = 200\,h$. For test case C, we used

$$c_0(t=0) = \frac{1}{2} + \frac{1}{2}\mathrm{erf}\left(\frac{y}{L_{\mathrm{c,ini}}}\right). \tag{25}$$

It can be shown that this form is a solution to a 2D diffusion problem. Here, we have chosen $L_{\mathrm{c,ini}} = 550\,h$.

The transient advection-diffusion equation for the concentration field is solved utilizing the in-built solvers in Comsol, namely the direct solver *MUMPS*, and the implicit time-stepping solver *generalized alpha*. The *amplification factor for high frequencies* is set to 0.75, and the *relative tolerance* to 1×10^{-3}. Since the damping is reduced compared to other implicit solvers at the cost of stability, we utilized this solver to capture gradients in the concentration field

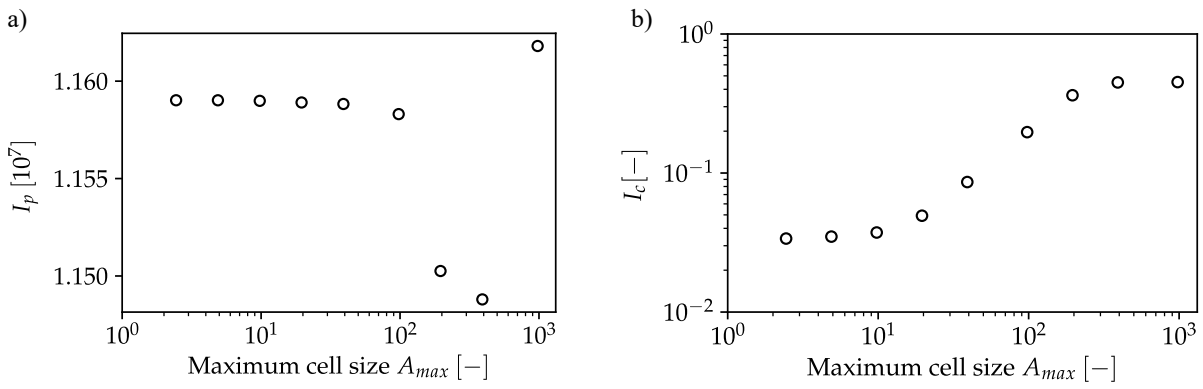

Figure 2: Convergence study for the maximum element size of the 2D model in the test case C. a) The global measure I_p of the flow equations converges to a fixed value. b) The mixing intensity I_c at the final timestep $t = 918\,T_{\text{dif,h}}$ converges to a fixed value as well. The final mesh utilized is the second-most refined.

more accurately and prevent numerical over-damping (COMSOL Multiphysics, 2019). The *intermediate timestepping* method is used, automatically choosing the time-step size, with a maximum time step of $\Delta t_{\max} = 23.5\,T_{\text{dif,h}}$.

For the flow problem, we have performed a convergence study with varying maximum size of the computational cells. We varied the *maximum cell size* as shown in figure 2, and as an indicator characterizing the solution we used the integral of the local pressure deviation from the mean, i.e.

$$I_p = \int (p - p_{\text{avg}})\mathrm{d}A, \tag{26}$$

where p_{avg} denotes the average pressure in the domain, and A denotes the area of the 2D domain. As can be seen from figure 2(a), the indicator converges to an asymptotic value when the cell size is reduced (i.e. the number of cells increases).

To check the convergence for the computation of the concentration field, we have also performed simulations with several maximum cell sizes. In figure 2(b), we show the resulting mixing intensity I_c, which is analogous to equation 20, i.e.

$$I_c = 1 - \frac{\int \left|c(t) - c_{\text{avg}}\right| \mathrm{d}A}{\int \left|c(0) - c_{\text{avg}}\right| \mathrm{d}A}. \tag{27}$$

As for the flow equations, the mixing intensity converges to an asymptotic value with decreasing maximum cell size. For very large cell sizes, the results are unphysical and show a strong overprediction of mixing.

S5 Test case C: Mixing regions

In figure 3, the regions of concentrations between $0.1 < c < 0.5$ are marked. These regions are indicative of the ability of the model to capture the dispersive broadening of material interfaces over time.

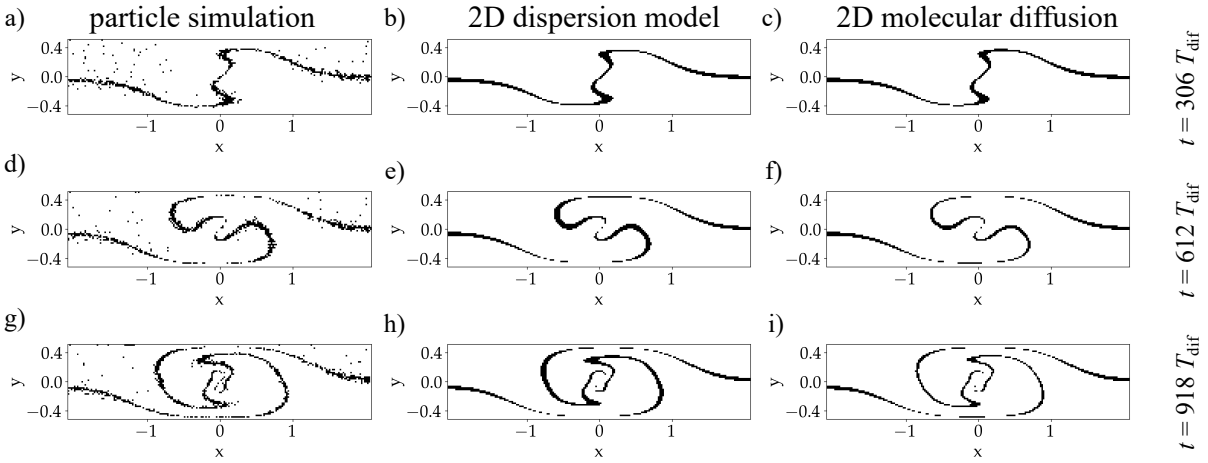

Figure 3: Comparison of mixing zones inside a Hele-Shaw cell as computed using 3D particle simulations (a,d,g), the 2D dispersion model (b,e,h) and pure 2D molecular diffusion (c,f,i). Shown are the regions with concentrations within the interval $0.1 < c < 0.5$. The resulting transition zones of the 3D particle simulations and the dispersion model show good agreement. At early times, the dispersion model and molecular diffusion generate similar profiles. Once the material interface passes the regions of enhanced dispersion, the width of the mixing zones increases.

References

BALAKOTAIAH, V., CHANG, H.-C. & SMITH, F. T. 1995 Dispersion of chemical solutes in chromatographs and reactors. *Philosophical Transactions of the Royal Society of London. Series A: Physical and Engineering Sciences* **351** (1695), 39–75.

COMSOL MULTIPHYSICS 2019 *COMSOL multiphysics reference manual, version 5.5*.

WOODING, R. A. 1960 Instability of a viscous liquid of variable density in a vertical Hele-Shaw cell. *Journal of Fluid Mechanics* **7** (4), 501–515.